Rate Coefficients and Mechanistic Analysis for the Reaction of Hydroxyl Radicals with 1,1-Dichloroethylene and *trans*-1,2-Dichloroethylene over an Extended Temperature Range

Takahiro Yamada, Abdulaziz El-Sinawi, Masud Siraj, and Philip H. Taylor*

Environmental Sciences and Engineering Group, University of Dayton Research Institute, 300 College Park, Dayton, Ohio 43469-0132

Jingping Peng, Xiaohua Hu, and Paul Marshall

Department of Chemistry, University of North Texas, P.O. Box 305070, Denton, Texas 76203-5070

Received: March 8, 2001; In Final Form: June 7, 2001

Rate coefficients are reported for the gas-phase reaction of the hydroxyl radical (OH) with 1,1-dichloroethylene (k_1) and *trans*-1,2-dichloroethylene (k_2) over an extended temperature range at 740 ± 10 Torr in a He bath gas. Absolute rate measurements were obtained using a laser photolysis/laser-induced fluorescence (LP/LIF) technique under slow flow conditions. Rate measurements for k_1 exhibited complex behavior with negative temperature dependence at temperatures below 640 K, a rapid falloff in rate between 650 and 700 K, and positive temperature dependence from 700 to 750 K. The simple Arrhenius equation adequately describes the data below 640 K and above 700 K and is given (in units of cm^3 molecule^{-1} s^{-1}) by $k_1(291-640\ \text{K}) = (1.81 \pm 0.36) \times 10^{-12} \exp(511 \pm 71)/\text{T}$ and $k_1(700-750\ \text{K}) = 3.13 \times 10^{-10} \exp(-5176/T)$. Rate measurements for k_2 also exhibited complex behavior with a near-zero or slightly negative temperature dependence below 500 K and a near-zero or slightly positive temperature dependence above 500 K. The modified Arrhenius equation adequately describes all of the data and is given (in units of cm^3 molecule^{-1} s^{-1}) by $k_2(293-720\ \text{K}) = (9.75 \pm 1.14) \times 10^{-18}\ T^{1.73\pm 0.05} \exp(727 \pm 46)/T$. Error limits are 2σ values. The room-temperature values for k_1 and k_2 are within $\pm 2\sigma$ of previous data using different techniques. The rate measurements were modeled using QRRK theory. OH addition to the unsubstituted carbon followed by adduct stabilization describes the low-temperature measurements for k_1. Analysis of equilibration in this system yields a C−O bond dissociation enthalpy of 32.8 ± 1.5 kcal mol^{-1} at 298 K, a value confirmed by ab initio calculations. OH addition followed by Cl elimination described the experimental data for k_2. Ab initio based transition state calculations for the H atom abstraction channel indicated that this mechanism is consistent with the rate measurements for k_1 above 700 K. The H abstraction channel for k_2 could not be observed because of the presence of a more rapid Cl elimination channel at elevated temperatures. H abstraction is predicted to be the dominant reaction channel for both k_1 and k_2 at flame temperatures.

Introduction

The dichloroethylenes represent significant organochlorine emissions to the environment. Vinylidene chloride (1,1-$C_2H_2Cl_2$) is used industrially for the production of poly(vinyl dichloroethylene) (PVDC) and 1,1,1-trichloroethane and was produced at a worldwide rate of 200 000 metric tons in 1985.[1] Vinylidene chloride is classified as a possible human carcinogen by the Integrated Risk Information System of the EPA.[2] 1,2-dichloroethylene is of little industrial importance but is nonetheless significant environmentally because it is a byproduct of chloroethylene manufacture.[1] High-temperature incineration remains the best available technology for the complete and permanent disposal of these hazardous materials. An important process contributing to the initial destruction of halogenated hydrocarbons under both atmospheric and combustion conditions is reaction with OH radicals.[3,4]

Previous measurements of the reaction of OH with 1,1- and 1,2-dichloroethylene were limited to low temperatures (220−432 K).[1,5−8] Arrhenius parameters derived from the previous studies are summarized in Tables 1 and 2 for 1,1-dichloroethylene and 1,2-dichloroethylene, respectively.

TABLE 1: Arrhenius Parameters from Previous Rate Measurements − 1,1-Dichloroethylene

$10^{12} \times$ A (cm^3 molecule^{-1} s^{-1})	E_a (cal mol^{-1})	T (K)	technique	ref
2.30 ± 0.44	−938 ± 209	240−400	FP−RF	7
1.6 ± 0.6	−1113 ± 219	297−368	DF−LIF	8
0.225 ± 0.027	−2271 ± 95.6	298−432	DF−MS	1

TABLE 2: Arrhenius Parameters from Previous Rate Measurements − 1,2-Dichloroethylene

$10^{12} \times$ A (cm^3 molecule^{-1} s^{-1})	E_a (cal mol^{-1})	T (K)	technique	ref
0.937 ± 1.47	−562 ± 169	240−400	FP−RF	7
2.1 ± 0.8	−40 ± 238	297−367	DF−LIF	8

The reaction mechanism is presumed to be addition to the π electrons associated with the C=C double bond. Edney et al.[5] measured the room-temperature rate constant for OH reaction with vinylidene chloride using the relative rate method. The rate constant observed (14.9×10^{-12} cm^3 molecule^{-1} s^{-1}) appeared to be anomalously high compared to reported values

* To whom correspondence should be addressed. Fax: (937) 229−2503, e-mail: taylorph@udri.udayton.edu.

10.1021/jp0109067 CCC: $20.00
Published on Web 07/17/2001

for the other chloroethylenes ($0.2-8.1 \times 10^{-12}$ cm^3 molecule^{-1} s^{-1}).[9] Using a similar experimental approach, Tuazon et al.[6] examined the room-temperature rate constant for OH reaction with 1,1- and 1,2-dichloroethylenes. However, in these studies, experiments were performed with and without a Cl atom scavenger (ethane). Plots of 1,1- and 1,2-dichloroethylene versus dimethyl ether (reference compound) consumption indicated that secondary processes contributed to substrate loss. As a result, the OH rate constants were obtained using the Cl atom scavenger and rates of 8.11 and 1.80×10^{-12} cm^3 molecule^{-1} s^{-1} were observed for 1,1- and *trans*-1,2-dichloroethylene, respectively. Product analyses using FTIR spectroscopy confirmed that secondary reaction chemistry involving Cl atoms was important for both substrates.

Kirchner et al.[1] measured the kinetics and reaction products from OH reactions with 1,1-dichloroethylene at low temperatures (298−432 K) and pressures of ∼1 Torr using electron impact mass spectrometry. The observed product distributions were complex and indicated that Cl elimination was insignificant. The mass spectral ions were furthermore indicative of a reaction mechanism involving primarily OH addition to the CH_2 side of the substrate. This is consistent with the absence of Cl elimination, which is only expected when the OH radical attacks the CCl_2 side or migrates there from the CH_2 side. Zhang et al.[7] measured the kinetics of the reaction of OH radicals with 1,1- and 1,2-dichloroethylene from 240 to 400 K using the flash photolysis−resonance fluorescence technique. The reactions were observed to be independent of pressure over a range of 5−50 Torr of argon. Their rate measurements for the dichloroethylenes (11.2 and 2.50×10^{-12} cm^3 molecule^{-1} s^{-1} for 1,1- and *trans*-1,2-dichloroethylene, respectively) compared to that of ethylene (8.06×10^{-12} cm^3 molecule^{-1} s^{-1})[9] indicated that the chlorine atom deactivates the carbon on which it is attached toward OH attack while activating the carbon on the other side of the double bond. Abbatt and Anderson[8] measured the kinetics of the reaction OH radicals with 1,1- and 1,2-dichloroethylene from 297 to 367 K using the discharge flow method coupled with laser-induced fluorescence detection. The reactivity of the chloroethylenes was observed to be considerably less than that of unsubstituted olefinic hydrocarbons when considered in terms of the alkenes ionization potentials. This was rationalized in terms of molecular orbital theory and the fact that the highest occupied molecular orbital is composed of carbon−carbon π bonding and halogen atom lone-pair contributions. The attacking OH radical experiences greater nonbonding interactions in the transition state than it does in the OH/alkene reactions, where the HOMO is solely carbon−carbon π bonding.

Given the lack of available data above 430 K, knowledge of the reaction rate constants and reaction mechanisms over an extended temperature range is essential to accurately predicting the combustion behavior of these compounds. Of specific interest to the dichloroethylenes is the relative importance of adduct stabilization, Cl elimination, and H abstraction. In this manuscript, we present absolute rate coefficients for the reaction of OH with 1,1-$C_2H_2Cl_2$ (k_1) and 1,2-$C_2H_2Cl_2$ (k_2) at atmospheric pressure over an extended temperature range:

$$1,1\text{-}C_2H_2Cl_2 + OH \rightarrow \text{products} \qquad (k_1)$$

$$1,2\text{-}C_2H_2Cl_2 + OH \rightarrow \text{products} \qquad (k_2)$$

Arrhenius parameters are derived from the data. A comparison of these measurements with prior measurements at lower temperatures and pressures is discussed. Ab initio calculations were performed to estimate thermodynamic properties, enthalpies of formation, entropies, and heat capacities. QRRK calculations were also performed to calculate energy dependent rate constants, $k(E)$, using the above thermodynamic properties. The most likely reaction mechanisms based on the ab initio and QRRK modeling of these reaction systems and their consistency with the available experimental data are discussed.

Experimental Approach and Data Reduction

The experimental procedures developed for LP-LIF studies of the reaction of OH radicals with chloroethylenes have been previously published.[10−12] A brief summary is given in the following paragraphs.

To minimize substrate photolysis at wavelengths <300 nm, HONO was used as a hydroxyl radical source. Parts per million concentrations of pure HONO (>99%) were generated as described by Febo et al.[13] and Brust et al.[14] HONO dissociates primarily into NO and OH when exposed to near-UV radiation of 351 nm. A competing dissociation channel, production of NO_2 and H atoms, has been observed to be negligible under similar experimental conditions.[15] A XeF excimer laser (Lamba Physik Compex model 102) was used as the photodissociation source. Initial $[OH]_0$ ranged from $\sim 3 \times 10^{10}$ to 9×10^{10} molecules cm^{-3} and was determined based on the measured excimer fluence (9−18 mJ cm^{-2}), the most recent published value of the absorption cross-section for HONO, 1.54×10^{-19} cm^2/molecule at 351 nm,[14] a quantum yield of unity,[16] and measured values of $[NO_2^-]$ taken to represent [HONO] determined using ion chromatography [$\sim(1-3) \times 10^{13}$ molecules cm^{-3}].

Initial substrate concentrations in the reactor, based on measured flow rates, ranged from $\sim 3 \times 10^{13}$ to $\sim 1 \times 10^{15}$ molecules cm^{-3}. The absence of adsorption on the injector probe (coated with boric acid) and reactor walls was verified using GC/MS analysis. All experiments were conducted at a total pressure of 740 ± 15 Torr. Samples of 1,1- and 1,2-dichloroethylene (99.9% purity) were obtained from Aldrich. GC/MS analyses indicated that this purity was met or exceeded.

The rate of disappearance of the OH may be presented as

$$-\mathrm{d[OH]/dt} = k[A_0][\mathrm{OH}] + k_d[\mathrm{OH}]$$

where k = bimolecular rate constant, A_0 = substrate concentration, and k_d = first-order rate for the reaction of OH with HONO and also includes diffusion out of the reaction volume. This relationship holds in the absence of any secondary reactions that may form or deplete OH. Solution of this equation yields $[\mathrm{OH}] = [\mathrm{OH}]_0 \exp -(k't)$, where $k' = k + k_d$. For all experiments, reactive and diffusive OH radical decay profiles exhibited exponential behavior and were fitted by the following nonlinear expression:

$$[\mathrm{OH}] = [\mathrm{OH}]_0 \exp -(k't) + \gamma$$

where γ is the constant background signal level and t is the time delay between the laser pulses. Because the organic concentration was much greater than the [OH], pseudo first-order exponential OH decays were observed and the individual temperature-dependent rate constants were determined by $k' = k\,[\text{substrate}] + k_d$, where the bimolecular rate constant, k, is the slope of the least-squares fit of k' versus the organic concentration. OH decays were measured over two to three decay lifetimes over a time interval of 0.2−30.0 ms. Values of k_d measured before and after a rate determination were observed to be constant within experimental uncertainties, indicating that the HONO source was stable over the course of an experiment.

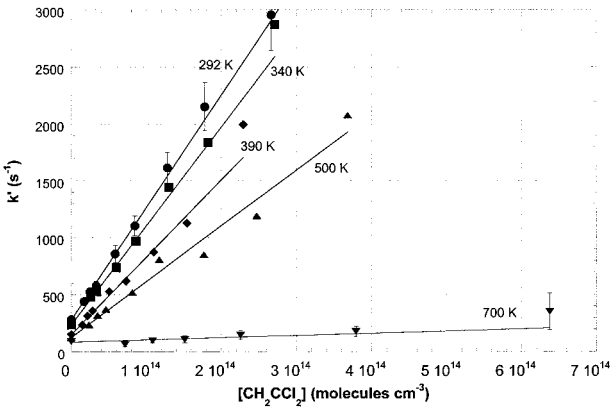

Figure 1. Plot of pseudo-first-order rate constants versus concentration for CH_2CCl_2 at five different reaction temperatures. Error bars for the 292 and 740 K data denote $\pm 2\sigma$ random error limits.

TABLE 3: Absolute Rate Coefficients (k_1) for OH + CH_2=CCl_2

T (K)	$10^{12}k_1$ (cm^3 molecule^{-1} s^{-1})	T (K)	$10^{12}k_1$ (cm^3 molecule^{-1} s^{-1})
291	10.01 ± 1.00[a]	550	4.45 ± 0.43
292	9.84 ± 0.37	600	3.96 ± 0.60
340	8.71 ± 0.37	640	4.14 ± 0.78
378	6.65 ± 0.86	680[b]	0.80 ± 0.38
383	6.67 ± 0.77	700	0.19 ± 0.02
390	6.80 ± 0.62	720	0.23 ± 0.03
440	5.70 ± 0.81	750	0.37 ± 0.13
500	4.90 ± 0.54		

[a] Errors represent $\pm 2\sigma$ and do not include the 5−10% uncertainty estimated for possible systematic errors. [b] OH decays at low substrate concentration exhibited biexponential character.

Numerical modeling indicated that the dominant source of OH decay in the absence of the substrate was the reaction with HONO ($k_{298} = 4.5 \times 10^{-12}$ cm^3 molecule^{-1} s^{-1}).[15] Typical values of k_d decreased from ~250 s^{-1} at low temperatures to ~100 s^{-1} at elevated temperatures, suggesting a reduction in the gas-phase concentration of HONO with increasing temperature. A plot of k' versus substrate concentration for 1,1-dichloroethylene at selected temperatures is shown in Figure 1.

Experimental Results

Rate data for k_1 and k_2 were obtained from ambient temperatures to ~750 K, under atmospheric pressure conditions. OH signals generated from the photolysis of HONO decreased below acceptable levels (S/N ratio <10) at higher temperatures, indicating significant thermal decomposition of HONO. The reduction in photolytically generated OH above 750 K was accompanied by an increase in background LIF, apparently because of the thermal generation of OH from the decomposition of HONO. Sources of secondary chemistry were not evident on the basis of chemical analysis of the gas stream containing the HONO precursors.[10] Concentrations of NO, NO_2, and HCl were below detection limits (<1.2×10^{12} molecules cm^{-3}). The OH consumption rate was thus controlled by the initial HONO concentration, which was maintained below 5×10^{13} molecules cm^{-3} to limit the first-order OH decay rate to <300 s^{-1}.

Absolute rate coefficients for k_1 and k_2 are presented in Tables 3 and 4, respectively. Random error limits ($\pm 2\sigma$) were below 15% at most temperatures. Rate measurements were collected for a wide range of initial concentrations and included an order of magnitude concentration difference for each series of runs. Substrate partial pressures were measured with a capacitance manometer. Substrate concentrations were based on total flow measurements checked before and after each rate measurement using the soap bubble method.

TABLE 4: Absolute Rate Coefficients (k_2) for OH + *trans*-CHCl=CHCl

T (K)	$10^{12}k_2$ (cm^3 molecule^{-1} s^{-1})	T (K)	$10^{12}k_2$ (cm^3 molecule^{-1} s^{-1})
293	2.24 ± 0.31[a]	610	2.08 ± 0.31
330	2.07 ± 0.27	650	2.17 ± 0.24
340	1.95 ± 0.13	660	2.31 ± 0.21
380	2.14 ± 0.18	700	2.33 ± 0.24
440	1.87 ± 0.19	720	2.32 ± 0.39
530	2.02 ± 0.24		

[a] Errors represent $\pm 2\sigma$ and do not include the 5−10% uncertainty estimated for possible systematic errors.

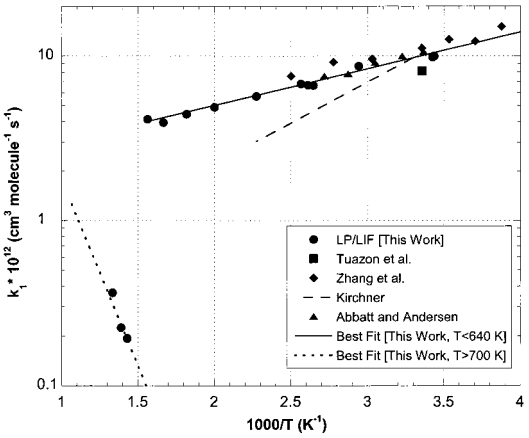

Figure 2. Arrhenius plot of kinetic data for k_1. Also shown are the results of previous studies (Tuazon et al.: $p = 1$ atm; bath gas, 80% N_2 and 20% O_2. Kirchner et al.: $p = 1-3$ Torr; bath gas, He. Abbatt and Anderson: $p = 55-85$ Torr; bath gas, N_2. Zhang et al.: $p = 35$ Torr; bath gas, Ar) and an Arrhenius fit to the data from this study (291−640 K and 700−750 K, $p = 740 \pm 10$ Torr).

All known rate measurements for k_1 are summarized in Figure 2. This work extends experimental measurement beyond the limit of ~400 K reported previously. A variety of techniques were used to collect these data. Examination of Figure 2 shows agreement at room temperature, within combined experimental uncertainties, between our work and that reported previously.[1,6−8] Rate measurements for k_1 exhibited complex behavior with negative temperature dependence at temperatures below 640 K, a rapid falloff in rate between 640 and 700 K, and an increase in rate above 700 K.

The simple Arrhenius equation adequately describes the data below 640 K and above 700 K, and is given (in units of cm^3 molecule^{-1} s^{-1}) by

$$k_1(291-640\ \text{K}) = (1.81 \pm 0.36) \times 10^{-12} \exp(511.3 \pm 71.0)/T$$

$$k_1(700-750\ \text{K}) = 3.13 \times 10^{-10} \exp(-5176/T)$$

Error limits for the low-temperature data are 2σ values. There is insufficient high-temperature data to calculate meaningful error limits. The negative activation energy derived from the Arrhenius fit to the data below 650 K is in good agreement with the previous studies of Zhang et al.[7] and Abbatt and Andersen[8] (<0.3 kcal mol^{-1} deviation). However, there is some discrepancy between our measurements and those of Kirchner et al.[1] (~1.7 kcal mol^{-1} deviation). It is possible that in the low-pressure measurements of Kirchner et al.,[1] rate measure-

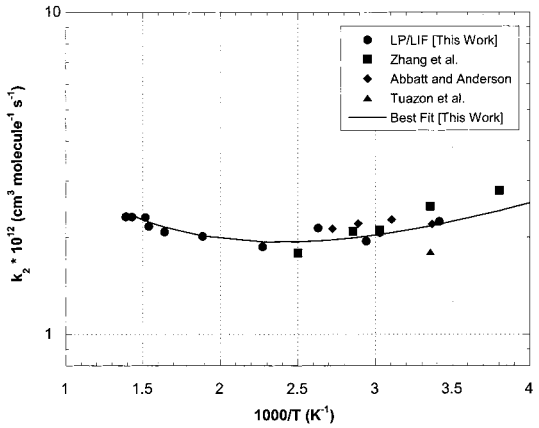

Figure 3. Arrhenius plot of kinetic data for k_2. Also shown are the results of previous studies (Tuazon et al.: $p = 1$ atm; bath gas, 80% N_2 and 20% O_2. Abbatt and Anderson: $p = 55-85$ Torr; bath gas, N_2. Zhang et al.: $p = 35$ Torr; bath gas, Ar) and a three-parameter modified Arrhenius fit to the data from this study (293−720 K, $p = 740 \pm 10$ Torr).

ments for k_1 were obtained under pressure falloff conditions (see the Modeling Results section).

All known rate measurements for k_2 are summarized in Figure 3. This work extends experimental measurements beyond the limit of ∼400 K reported previously. Examination of Figure 3 shows excellent agreement at room temperature (±10%) between our results and those reported previously by Zhang et al.[7] and Abbatt and Anderson.[8] The previous room-temperature rate measurements of Tuazon et al.[6] using the relative rate method were ∼18% lower than our measurements. Rate measurements for k_2 exhibited a slightly negative or near-zero temperature dependence below 500 K and a slightly positive or near-zero temperature dependence above 500 K. The modified Arrhenius equation yielded a better fit to the data than the simple Arrhenius expression and is given (in units of cm^3 molecule^{-1} s^{-1}) by

$$k_2(293-720\ \mathrm{K}) = (9.75 \pm 1.14) \times 10^{-18} T^{1.73\pm 0.05} \exp(727 \pm 46)/T$$

Error limits are 2σ values. The near-zero activation energy below 400 K is in good agreement with the previous studies of Abbatt and Andersen[8] (see Figure 3). Zhang et al.[7] reported a larger negative activation energy of ∼0.6 kcal mol^{-1}. However, the respective temperature dependencies of the study of Zhang et al.[7] and this study are statistically identical between 298 and 400 K.

Theoretical Approach

The composite ab initio calculation method, G3(MP2),[17] was used to calculate thermodynamic properties of reactants, intermediate radicals, transition states (TSs), and products with the Gaussian 94[18] and Gaussian 98[19] computer codes. The enthalpies of formation of the reactants were obtained from the literature.[20−22] The enthalpies of formation of intermediate radicals, TSs, and products were determined by the energy differences from the reactants, calculated by G3(MP2).[17] ZPE and thermal correction were incorporated to estimate enthalpies of formation at 298 K.[23] Entropy and heat capacity were calculated based on the geometry optimized with MP2(full)/6-31G(d), and frequencies were calculated with the HF/6-31G(d) level of theory using statistical mechanics. The internal rotational motions were treated as hindered rotors using the internal rotational treatment advanced by Pitzer and Gwinn.[24]

The rate coefficients for each pathway can be expressed, in general terms, using transition state theory (TST)[25] as shown below:

$$k = (k_b T/h) \exp(\Delta S^{\ddagger}/R) \exp(-\Delta H^{\ddagger}/RT) \qquad (1)$$

where h is Planck's constant, k_b is the Boltzmann constant, and $\Delta S^{\ddagger}$ is equal to $S^{\circ}_{298,\mathrm{TS}} - S^{\circ}_{298,\mathrm{reactant}}$. This expression is then fitted by three parameters, B, n, and C, over a temperature range of 200−2000 K, as expressed below:

$$k = B(T)^n \exp(-C/RT) \qquad (2)$$

QRRK analyses[26,27] for $k(E)$, combined with the modified β collision analysis of Gilbert et al.,[28] were used to predict the pressure-dependent rate constants.

Variational transition state theory (VTST) calculations were performed to estimate the rate constant for OH addition to 1,1- and *trans*-1,2-dichloroethylene at the high-pressure limit. The calculations were carried out as follows. First, the intrinsic reaction coordinates (IRCs) for the addition of OH to each end of the C═C bond were defined at the HF/6-31G(d,p) level near the saddle point region. At various fixed C−O separations along the IRCs, frequencies were obtained normal to the IRC, also at the HF/6-31G(d,p) level of theory. The results were scaled by a factor of about 0.9. (A factor of 0.901 was employed, derived from scaling to match observed frequencies for C_2H_4, C_2Cl_4, and OH.[21]) Then energies were computed at the spin-projected PMP4/6-311+G(d,p) level, relative to reactants.[18] These energies, geometries and frequencies were used to derive canonical TST rate constants as a function of position along the IRC. At each temperature, the VTST result was obtained by interpolation to find the minimum rate constant, i.e., the point where the Gibbs energy of activation is maximized.

These VTST results correspond to the high-pressure limit for OH addition, where the initially formed excited adduct is always stabilized by collisions. At finite pressures, some fraction of the excited adducts can dissociate back to reactants before collisional stabilization or fragmentation, and thus, the observed rate constant is likely to be smaller than the calculated one. At a given pressure, this effect will become more pronounced at elevated temperatures, because the reaction moves further from the high-pressure limit.

The variationally located transition states lie at C−O separations approximately 0.05 Å smaller than the local energy maxima along the IRCs. As may be seen from Figure 4 (top) for 1,1-dichloroethylene, the variational TS for β addition lies in a region approximately 2 kcal mol^{-1} below the reactants' energy, whereas α addition (at the CCl_2 end) requires overcoming a positive barrier of around +2 kcal mol^{-1}. The α addition channel is also found to be somewhat less favorable in an entropy context as well (the preexponential factor ($BT^n e^n$) is approximately 9 times smaller at 298 K, see Table 5). Figure 4 (bottom) shows the reaction path for OH addition to *trans*-1,2-dichloroethylene and indicates a significant computed barrier which is discussed in the following section.

The derived VTST rate constants are plotted in Figure 5. For 1,1-dichloroethylene, the α channel has a simple positive temperature dependence. The β channel is more important at all temperatures and has a more complex behavior. The negative relative transition state energy contributes to a negative temperature dependence for the rate constant, an effect which dominates at low temperatures, whereas increases in temperature

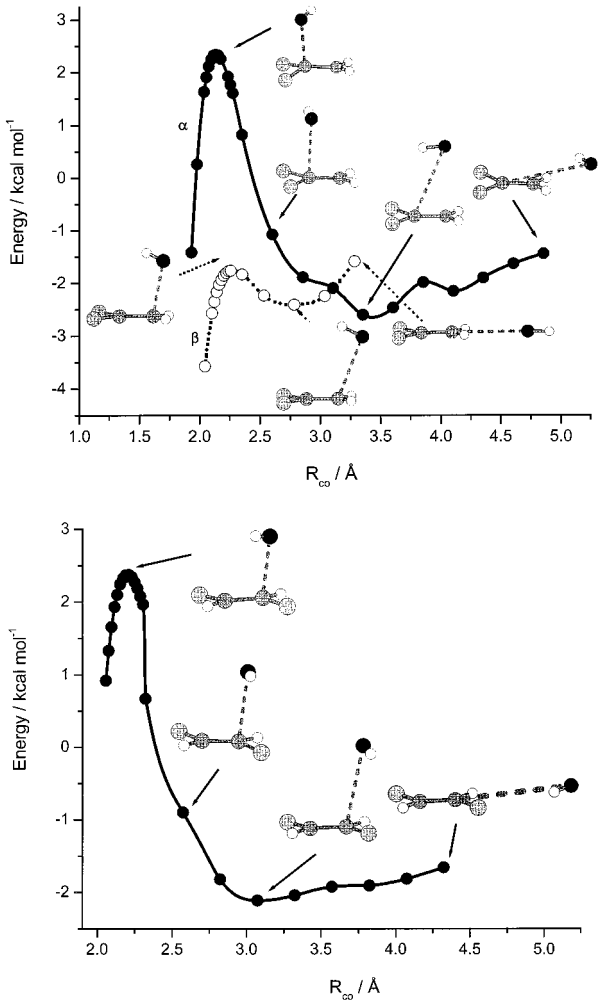

Figure 4. (top) Classical energies (no ZPE) relative to OH + CH_2CCl_2 for addition of OH at the CH_2 end (β site, open circles) and the CCl_2 end (α site, solid circles), calculated at the PMP4/6-311+G(d,p)//HF/6-31G(d,p) level of theory, together with molecular structures along the reaction path. (bottom) Classical energies (no ZPE) relative to OH + *trans*-CHClCHCl for addition of OH, calculated at the PMP4/6-311+G(d,p)//HF/6-31G(d,p) level of theory, together with molecular structures along the reaction path.

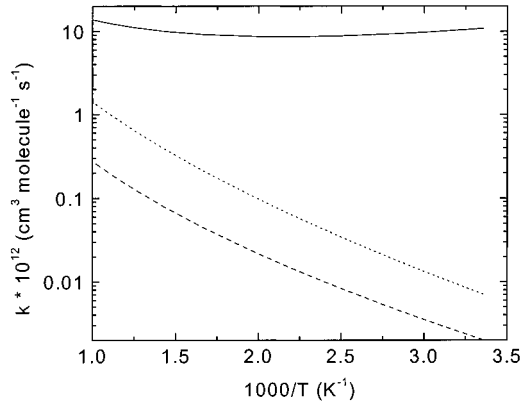

Figure 5. Ab initio high-pressure limit rate constants for the addition of OH to chlorinated ethylenes: solid line, OH + CH_2CCl_2 (α channel); dashed line, OH + CH_2CCl_2 (β channel); dotted line, OH + *trans*-CHClCHCl (see text). OH torsion about the forming C−O bond was treated as a vibrator.

more rapidly increase the partition function of the loose TS as compared to the reactants, leading to increasing rate constants at higher temperatures.

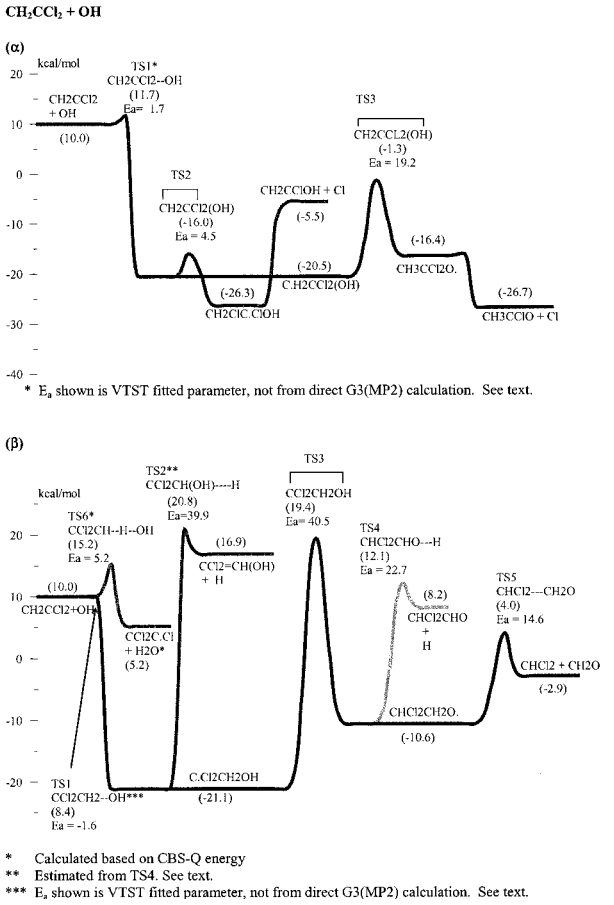

Figure 6. Potential energy diagrams for the OH addition to CH_2CCl_2. (a) α site, (b) β site. Energies are $\Delta H_f°_{298}$ in kcal mol^{-1}.

The rate constants for the reverse reactions, dissociation of adducts back to reactants, were calculated based on the VTST forward rate using the principle of microscopic reversibility.

Modeling Results

Thermodynamic properties of reactants, intermediate radicals, and TSs estimated based on G3(MP2) calculation results are given in Table 5. The activation energies for H atom abstraction reactions were calculated using both G3(MP2) and CBS-Q composite ab initio theory.[29] The activation energies for H atom abstraction reactions using G3(MP2) were 8.69 and 6.92 kcal/mol at 0 K for 1,1- and 1,2-dichloroethylene, respectively, whereas the CBS-Q calculation yielded values of 5.36 and 3.78 kcal/mol at 0 K for 1,1- and 1,2-dichloroethylene, respectively. The CBS-Q value was considered more accurate based on its consistency with the high-temperature 1,1-dichloroethylene data. G3(MP2) calculation results for all compounds which are involved in the reaction path analysis are given in Table 6. CBS-Q calculation results for the H atom abstraction reactions are also shown in Table 6.

Figures 6 and 7 present potential energy diagrams at 298 K for 1,1- and 1,2-dichloroethylene, respectively. Energy levels shown are based on G3(MP2) calculation results with the exception of the entrance channels, the H atom abstraction channels, and H atom dissociation to form CCl_2═CHOH (TS2 in Figure 6b). Because the TS2 energy level was calculated to be 0.7 kcal mol^{-1} lower than the product energy level, the activation energy obtained for an analogous reaction, i.e., the reverse of TS4 in Figure 6b (3.9 kcal mol^{-1}), was applied to TS2 and the energy level was thus estimated to be 20.8 kcal mol^{-1}. The entrance channel is based on the VTST calculation

TABLE 5: Thermodynamic Properties of Reactants, Intermediate Radicals, and TSs for the CH_2=CCl_2 + OH and CHCl=CHCl + OH Reaction System

	ΔH^f_0 [a]	$S(298)$ [b]	Cp(300) [c]	Cp(400)	Cp(500)	Cp(600)	Cp(800)	Cp(1000)	Cp(1500)	symmetry [d]	source
					CH_2CCl_2 + OH Alpha Channel						
CH2CCl2	−3.0 [e]	68.84	16.02	18.71	20.77	22.36	24.67	26.27	28.68	2	G3(MP2)
OH	9.3	43.88	7.17	7.09	7.06	7.06	7.15	7.33	7.44	1	ref 21
C.H2CCl2OH	−23.3	85.93	23.73	26.86	29.11	30.78	33.15	34.84	37.56	2	G3(MP2)
CH3CCl2O.	−18.9	78.92	21.66	24.91	27.52	29.62	32.78	35.01	38.34	3	G3(MP2)
CH2ClC.ClOH	−29.0	86.19	21.30	24.58	27.18	29.20	32.11	34.14	37.25	1	G3(MP2)
TS2 [f]	−18.7	81.41	21.31	24.40	26.78	28.63	31.32	33.24	36.25	1	G3(MP2)
TS3	−3.6	76.74	20.79	24.61	27.57	29.84	33.03	35.13	38.06	1	G3(MP2)
					CH_2CCl_2 + OH Beta Channel						
C.Cl2CH2OH	−23.8	83.91	21.72	25.10	27.68	29.65	32.47	34.43	37.42	2	G3(MP2)
CHCl2CH2O.	−13.1	82.29	20.70	24.33	27.24	29.51	32.80	35.08	38.40	1	G3(MP2)
TS2 [f]	13.2	86.57	23.78	27.12	29.42	31.03	33.14	34.53	36.63	1	G3(MP2)
TS3	17.1	78.09	19.57	23.30	26.38	28.83	32.33	34.66	37.86	1	G3(MP2)
TS4	9.4	83.36	22.28	25.80	28.45	30.44	33.19	34.99	37.53	1	G3(MP2)
TS5	1.2	84.58	21.36	24.50	26.97	28.88	31.68	33.66	36.66	1	G3(MP2)
TS6	11.7	86.18	23.88	27.11	29.44	31.15	33.5	35.06	37.39	1	CBS-Q
					CHClCHCl + OH						
CHClCHCl	−2.5 [g]	69.45	15.92	18.45	20.51	22.14	24.51	26.15	28.57	2	G3(MP2)
C.HClCHClOH	−26.7	86.82	21.73	25.04	27.60	29.55	32.33	34.28	37.30	1	G3(MP2)
CH2ClCHClO.	−16.5	82.85	20.54	24.21	27.14	29.42	32.73	35.01	38.33	1	G3(MP2)
CHCl2C.HOH	−23.2	86.45	21.51	24.76	27.31	29.27	32.13	34.13	37.22	1	G3(MP2)
TS2 [f]	−16.9	82.70	20.81	23.75	26.17	28.12	30.96	32.98	36.12	1	G3(MP2)
TS3	15.6	87.31	23.21	26.58	28.94	30.61	32.84	34.31	36.51	1	G3(MP2)
TS4	11.8	78.26	19.52	23.42	26.55	29.00	32.47	34.74	37.88	1	G3(MP2)
TS5	0.5	84.08	21.67	25.37	28.12	30.17	33.20	34.86	37.46	1	G3(MP2)
TS6	−8.7	84.96	21.35	24.66	27.16	29.06	31.80	33.73	36.67	1	G3(MP2)
TS7	10.6	86.65	23.68	26.77	29.10	30.84	33.28	34.90	37.31	1	CBS-Q

[a] Enthalpies of formation at 0 K, unit in kcal/mol. [b] Entropy at 298 K, unit in cal/mol K. [c] Heat capacity at $300 \le T/K \le 1500$, unit in cal/mol K. [d] Symmetry number included in the entropy calculation. [e] Estimated based on literature value of $\Delta H_f°_{298}$[22] and temperature correction 298−0 K calculated using HF/6-31G(d) determined frequencies scaled by 0.8929. [f] TS numbers correspond to potential energy diagrams in Figures 6 and 7. TS1 is not shown; the rate was calculated based on VTST (see text). [g] Estimated based on literature value of $\Delta H_f°_{298}$,[20] and temperature correction 298−0 K calculated using HF/6-31G(d) determined frequencies scaled by 0.8929.

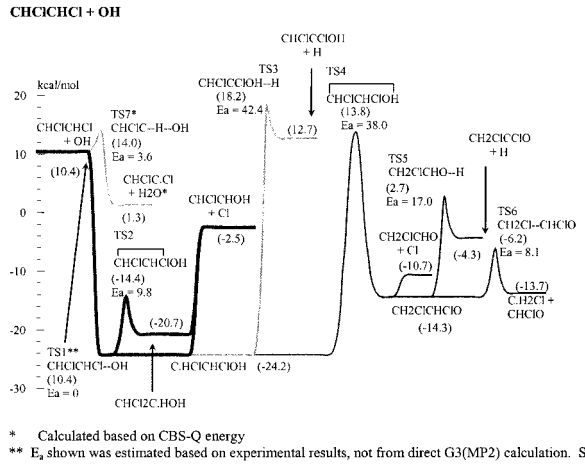

* Calculated based on CBS-Q energy
** E_a shown was estimated based on experimental results, not from direct G3(MP2) calculation. See text.

Figure 7. Potential energy diagrams for the OH addition to *trans*-CHClCHCl. Energies are $\Delta H_f°_{298}$ in kcal mol^{-1}.

results and the H atom abstraction channel is based on the CBS-Q calculation results.

Tables 7 and 8 present the high-pressure-limit Arrhenius parameters for the various OH addition reaction pathways for 1,1-dichloroethylene and *trans*-1,2-dichloroethylene, respectively. For *trans*-1,2-dichloroethylene, our energy calculations along the reaction coordinate yielded a large +2.5 kcal mol^{-1} classical barrier to reaction (see Figure 4b). This is incompatible with the observed rate constants and, for example, implies a room temperature rate constant nearly 3 orders of magnitude lower than that measured. We do not have a simple explanation for the overestimated barrier. Spin-projected PMP4/6-311+G-(d,p) theory works well for the other chlorinated ethylenes as seen in this work and elsewhere.[10−12] Potential sources of error include deficiencies in the correlation treatment and basis set size, but implementation of sufficiently high levels of theory is nontrivial. Preliminary studies at the QCISD(T)-based G3(MP2) level yielded an even higher barrier of about 3 kcal mol^{-1}, so presumably, much more demanding correlation treatments and/or basis sets are needed. Another source of error might be incorrect geometries along the reaction coordinate. However, for the simplest analogue, OH + C_2H_4, we have found that the HF/6-31G(d,p) values, as used here, closely match QCISD/6-311G(d,p) values (and do so much better than MP2-based geometries). Without a clear resolution of the origin of the qualitatively incorrect VTST rate constants for OH + *trans*-CHCl=CHCl, subsequent kinetic modeling of this reaction was instead based on a temperature-independent rate constant of 2.0×10^{-12} cm^3 molecule^{-1} s^{-1}. This value is a composite of all prior measurements of k_2 at low temperatures. Ab initio VTST data were employed for the entrance channels for the other pathways.

Figures 8 and 9 present a comparison of the experimental data with QRRK predictions in Arrhenius form at $p = 1$ atm for OH addition to 1,1-dichloroethylene and 1,2-dichloroethylene, respectively. For 1,1-dichloroethylene, the agreement between the overall forward rate for the β channel (represented exclusively by the stabilization rate) and the experimental data is excellent between 293 and 640 K. The reverse reaction begins to dominate above 650 K and is responsible for the rapid drop-off in the observed bimolecular rate coefficients between 640 and ~700 K. The well depth for the β-channel was reduced by

TABLE 6: Calculated Energy of Reactant, Intermediate Radicals, and Products at 0 K[a]

	G3(MP2)	CBS-Q
	CH2CCl2 + OH	
	Alpha Channel	
CH2CCl2	−996.75312	−996.73466
OH	−75.65469	−75.64887
C.H2CCl2OH	−1072.45502	
CH3CCl2O.	−1072.44796	
CH2ClC.ClOH	−1072.46400	
CH2CClOH	−612.74403	
CH3CClO	−612.77840	
H	−0.50184	
Cl	−459.68724	
TS1	−1072.40189	
TS2	−1072.44758	
TS3	−1072.42362	
	CH_2CCl_2 + OH	
	Beta Channel	
C.Cl2CH2OH	−1072.45579	
CHCl2CH2O.	−1072.4387	
CCl2CHOH	−1071.89554	
CHCl2CHO	−1071.9091	
CH2O	−114.35303	
C.HCl2	−958.0752438	
CCl2C.H	−996.07095	−996.05536
H2O	−76.34241	−76.33648
TS1	−1072.40777	
TS2	−1072.4029	
TS3	−1072.39067	
TS4	−1072.4029	
TS5	−1072.41594	
TS6	−1072.393966	−1072.37499
	CHClCHCl + OH	
CHClCHCl	−996.75284	−996.73471
C.HClCHClOH	−1072.46101	
CH2ClCHClO.	−1072.44474	
CHCl2C.HOH	−1072.45542	
CHClCHOH	−612.74013	
CHClCClOH	−1071.90162	
CH2ClCHO	−612.75311	
CH2ClCClO	−1071.92910	
CHClO	−573.53045	
C.H2Cl	−498.91605	
CHClC.Cl	−996.07837	−996.06222
TS1	−1072.40501	
TS2	−1072.44537	
TS3	−1072.39352	
TS4	−1072.39970	
TS5	−1072.41766	
TS6	−1072.43222	
TS7	−1072.39650	−1072.37756

[a] Unit in Hartree. TS numbers correspond to potential energy diagrams in Figures 6 and 7.

2 kcal mol^{-1} to improve the fit to the data above 500 K. This is well within the uncertainty of the ab initio calculations and is consistent with an estimate of the enthalpy of formation of the $CH_2(OH)CCl_2$ adduct based on equilibrium considerations observed in the experimental measurements between 640 and 700 K (see below). For 1,2-dichloroethylene, the excellent agreement between the overall forward rate (the sum of the stabilization and chlorine elimination channels) and the experimental data is fortuitous because of the lack of any substantial temperature dependence in the measurements.

Figure 8 also shows the QRRK estimated temperature-dependent reaction rate constants for 1,1-dichloroethylene. The predicted dominant product is CCl_2CH_2OH, the stabilized product formed by OH addition to the β site. OH addition to the α site becomes important above 1000 K. Above 1000 K, OH addition to the α site followed by Cl elimination leads to

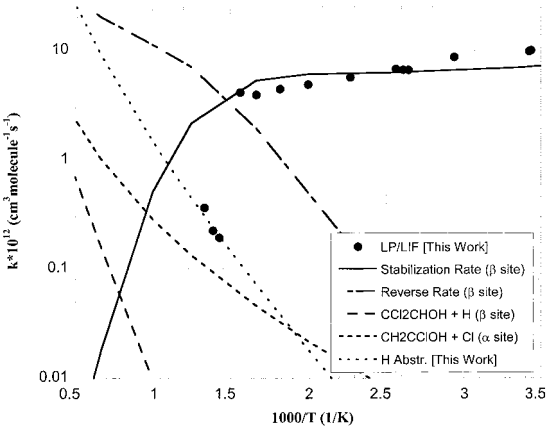

Figure 8. Comparison of experimental results with the QRRK model results for k_1 (p = 1 atm). Shown are the stabilization rate, reverse rate and H elimination channel for the β site, and the chlorine elimination channel for the α site. Also shown is the ab initio based TST calculation of the H-atom abstraction channel.

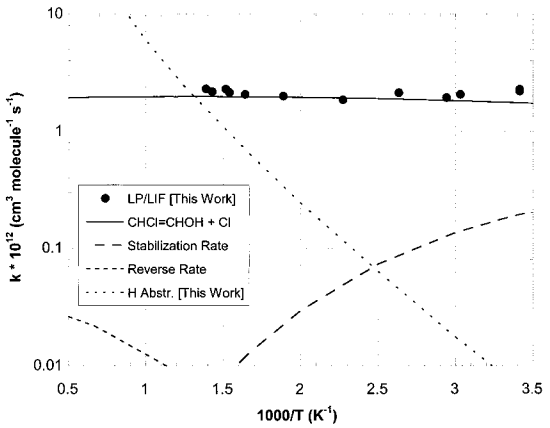

Figure 9. Comparison of experimental results with the QRRK model results for k_2 (p = 1 atm). Shown are the chlorine elimination rate, stabilization rate, reverse reaction, hydrogen elimination channel, and the ab initio based TST calculation of the H-atom abstraction channel.

the formation of CH_2═CClOH. At temperatures approaching 2000 K, OH addition to the β site followed by H elimination produces CCl_2═CHOH. The rate of formation of these chemically activated reaction products is small compared to the predicted rate of H-atom abstraction (see below). It should be noted that α and β addition pathways can only be considered separately if OH migration between the carbon atoms does not occur.

Figure 9 also illustrates the QRRK estimated temperature-dependent reaction rate constants for 1,2-dichloroethylene. The dominant product is CHCl═CHOH, formed by OH addition followed by Cl atom elimination. The stabilization reaction accounts for <10% of the overall rate at room temperature and becomes less significant at higher temperatures. The reverse of OH addition is insignificant under all reaction conditions.

Figures 8 and 9 also present TST calculations for the respective H-atom abstraction channels for 1,1-dichloroethylene and 1,2-dichloroethylene, respectively. For 1,1-dichloroethylene, a CBS-Q composite ab initio calculation yielded an activation energy of 5.16 kcalmol^{-1}. A <1 kcal mol^{-1} barrier increase and the entropy of activation calculated from the ab initio-based geometry of the transition state yield a rate (see Table 5) that is in good agreement with the experimental measurements between 700 and 750 K. This contrasts with the QRRK-based Cl elimination channel (OH attack at the α site) that is a factor

TABLE 7: QRRK Input Parameters Rate Constants for OH Addition to CH_2=CCl_2

A. α site[a]

reaction	*B* (s^{-1} or cm^3/(molecule))	*n*	*C* (kcal mol^{-1})
1 $CH_2CCl_2 + OH \rightleftharpoons C\bullet H_2CCl_2(OH)$	3.26×10^{-20}	2.44	1.73
−1 $C\bullet H_2CCl_2(OH) \rightleftharpoons CH_2CCl_2 + OH$[b]	1.19×10^{10}	0.82	32.60
2 $C\bullet H_2CCl_2OH \rightleftharpoons CH_2ClC\bullet Cl(OH)$	3.04×10^{11}	0.23	4.80
−2 $CH_2ClC\bullet Cl(OH) \rightleftharpoons C\bullet H_2CCl_2OH$	9.73×10^{9}	0.82	10.40
3 $C\bullet H_2CCl_2(OH) \rightleftharpoons CH_3CClO + Cl$	6.39×10^{8}	0.77	19.06
4 $CH_2ClC\bullet ClOH \rightleftharpoons CH_2CClOH + Cl$[c]	3.90×10^{13}	0.00	18.70
5 $C\bullet H_2CCl_2(OH) \rightleftharpoons CH_2CClOH + Cl$[c]	3.90×10^{13}	0.00	24.50

B. β site[d]

reaction	*B* (s^{-1} or cm^3/(molecule/s))	*n*	*C* (kcal mol^{-1})
1 $CCl_2CH_2 + OH \rightleftharpoons C\bullet Cl_2CH_2(OH)$	5.28×10^{-18}	2.00	−1.60
−1 $C\bullet Cl_2CH_2(OH) \rightleftharpoons CCl_2CH_2 + OH$[b]	3.02×10^{7}	2.11	26.48
2 $C\bullet Cl_2CH_2OH \rightleftharpoons CHCl_2CH_2O\bullet$	2.96×10^{8}	0.81	40.80
−2 $CHCl_2CH_2O\bullet \rightleftharpoons C\bullet Cl_2CH_2OH$	1.78×10^{10}	0.70	30.13
3 $C\bullet Cl_2CH_2(OH) \rightleftharpoons CCl_2CH(OH) + H$	5.83×10^{11}	0.65	38.02
4 $CHCl_2CH_2O\bullet \rightleftharpoons CHCl_2CHO + H$	9.81×10^{9}	1.41	22.70
5 $CHCl_2CH_2O\bullet \rightleftharpoons C\bullet HCl_2 + CH_2O$	2.29×10^{12}	0.51	15.08
6 $CCl_2CH_2 + OH \rightleftharpoons CCl_2$=$C\bullet H + H_2O$	3.06×10^{-17}	2.00	6.00

[a] Grouped geometric mean frequencies of the adduct with effective degeneracies: 361.2 cm^{-1} (9.376), 1137.1 cm^{-1} (4.688), 3270.5 cm^{-1} (2.936). Lennard-Jones parameters: CH_2CCl_2OH adduct, $\sigma = 5.198$ Å, $\epsilon/k = 533.08$ K; He bath gas, $\sigma = 2.576$ Å, $\epsilon/k = 470.00$ K. [b] Rate was estimated based on forward rate constant and principle of microscopic reversibility. [c] Arrhenius A factor for Cl elimination reaction was adopted from the reaction: $C_2H_4Cl \rightarrow C_2H_4 + Cl$, ref 33. [d] Grouped geometric mean frequencies of the adduct with effective degeneracies: 150.0 cm^{-1} (4.327), 710.1 cm^{-1} (8.386), 2178.9 cm^{-1} (4.287). Lennard-Jones parameters: CCl_2CH_2OH (adduct), $\sigma = 5.198$ Å, $\epsilon/k = 533.08$ K; He (bath gas), $\sigma = 2.576$ Å, $\epsilon/k = 470.00$ K.

of 4 lower than experimental measurements above 700 K. Experiments where Cl atoms were intentionally generated from the 193 nm photolysis of 1,1-dichloroethylene suggest that the Cl atom elimination channel is not attributable to the experimental data above 700 K. The Cl atoms result in a series of secondary reactions that resulted in an effective bimolecular rate constant on the order of $6 \pm 1 \times 10^{-13}$ cm^3 $molecule^{-1}$ s^{-1}. This rate was observed to be temperature-independent between 700 and 900 K. Kinetic isotope measurements for 1,1-dichloroethylene at 720 K were inconclusive and were not repeated because of the high cost of the deuterated standard. For 1,2-dichloroethylene, a similar CBS-Q composite ab initio calculation yielded an activation energy for this reaction of 3.6 kcal mol^{-1}. This barrier and the entropy of activation calculated from the ab initio-based geometry of the transition state yield a rate (see Table 6) that is a factor of 40 lower than experimental measurements at 400 K and a factor of 2 lower than experimental measurements at 720 K. These calculations (and the experimental measurements for 1,2-dichloroethylene) indicate that the H-atom abstraction channel is not important below temperatures of ~800 K. At higher temperatures, H abstraction is the dominant OH reaction mechanism for both of these chloroethylenes.

The predicted reaction mechanism for 1,1-dichloroethylene is consistent with the low temperature product analysis previously reported by Kirchner et al.[8] The dominant reaction product was the stabilized adduct from OH attack at the β site. There was little evidence for Cl atom elimination reactions. The only previous product study for 1,2-dichloroethylene involved the smog chamber study of Tuazon et al.[6] FTIR measurements indicated that Cl elimination reactions were occurring. However, the experimental conditions of the smog chamber experiments are more complex than those modeled in this study, and a direct comparison of observed reaction products with the QRRK-predicted results presented here is not valid.

Figure 10 illustrates the effect of pressure on the QRRK estimated adduct stabilization reaction (and the reverse) for 1,1-dichloroethylene. The modeling results indicate that all prior measurements (including this study) were obtained in the falloff region at temperatures at and above room temperature. Prior measurements of this reaction (typically at room temperature) at pressures ranging from ~1−5 Torr[1] to ~25−50 Torr[8] did not exhibit pressure effects. This was likely due to a lack of sufficient accuracy to resolve the QRRK predicted 10 to 20% change in rate constant with increasing pressure at these low temperatures. As shown in Figure 10, the larger negative temperature dependence observed in the measurements of Kirchner et al.[1] can be explained because of pressure effects.

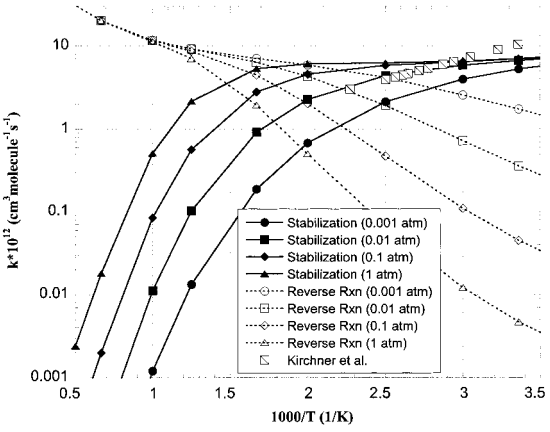

Figure 10. Arrhenius plot of the QRRK model results for k_1 at 0.001, 0.01, 0.1, and 1 atm. Shown are the adduct stabilization channel and the reverse reaction for the β site.

The crossover between stabilization and reverse (redissociation) channels shown in Figure 10 indicates that equilibration for the addition channel

$$CH_2{=}CCl_2 + OH \leftrightarrow CH_2(OH){-}CCl_2 \quad (k_{1a},k_{-1a})$$

becomes important in the 600−700 K regime, consistent with the sharp drop observed in the total rate constant k_1. The decays

TABLE 8: QRRK Input Parameters Rate Constants for OH Addition to *trans*-CHCl=CHCl[a]

reactions	*B* (s^{-1}or cm^3/(molecule s))	*n*	*C* (kcal mol^{-1})
1 CHClCHCl+OH → C•HClCHCl(OH)	2.00×10^{-12}	0.00	0.00
−1 C•HClCHCl(OH) → CHClCHCl+OH[b]	1.44×10^{20}	−2.13	35.76
2 C•HClCHCl(OH) → CCl_2HC•H(OH)	2.43×10^{11}	0.33	10.21
−2 CCl_2HC•H(OH) → C•HClCHCl(OH)	1.65×10^{11}	0.41	6.67
3 C•HClCHCl(OH) → $CH_2ClCHClO$•	3.33×10^{12}	0.92	38.32
−3 $CH_2ClCHClO$• → C•HClCHCl(OH)	7.58×10^{9}	0.79	28.37
4 C•HClCHCl(OH) → CHCl=CHOH+Cl	3.90×10^{13}	0.00	21.70
5 C•HClCHCl(OH) → CHCl=CClOH+H	6.87×10^{9}	1.24	42.43
6 $CHCl_2C$•HOH → CHCl=CHOH + Cl[c]	3.90×10^{13}	0.00	18.18
7 CHClCHCl+OH → C•ClCHCl + H_2O	3.10×10^{-17}	2.00	3.60

[a] Grouped geometric mean frequencies of the adduct with effective degeneracies: 338.7 cm^{-1} (7.46), 1110.1 cm^{-1} (6.52), 3222.0 cm^{-1} (3.02). Lennard-Jones parameters: CHClCHClOH (adduct), $\sigma = 5.327$ Å, $\epsilon/k = 469.42$ K; He (bath gas), $\sigma = 2.576$ Å, $\epsilon/k = 470.00$ K. [b] Rate was estimated based on forward rate constant and principle of microscopic reversibility. [c] Arrhenius A factor for Cl elimination reaction was adopted from the reaction: $C_2H_4Cl \rightarrow C_2H_4 + Cl$, ref 33.

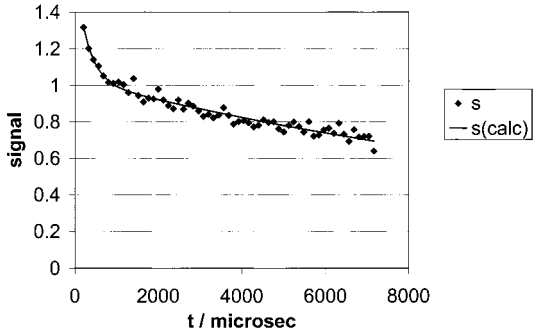

Figure 11. Biexponential OH decay and resulting fit to the data using reactions k_{1a}, k_{-1a}, and k_d and eq 3 (see text). $T = 680$ K, $[CH_2CCl_2]_0 = 3.35 \times 10^{14}$ molecules cm^{-3}.

at 680 K, in the middle of the drop-off region, show modest deviations from simple exponential behavior. If they are forced to fit pseudo-first-order kinetics, the resulting k_1 value lies between the values at 640 and 700 K (see Table 3). For a more detailed analysis of the equilibration region, we considered the following mechanism:

$$\mathrm{OH} + \mathrm{CH_2CCl_2} \rightarrow \mathrm{adduct} \quad k_{1a}$$

$$\mathrm{adduct} \rightarrow \mathrm{OH} + \mathrm{CH_2CCl_2} \quad k_{-1a}$$

$$\mathrm{OH} \rightarrow \mathrm{loss} \quad k_d$$

This is a simplified form of a similar mechanism analyzed by Wine and co-workers,[30] and the corresponding expression for the fluorescence signal S_t is

$$S_t = \text{background} + S_0 \frac{(k_{-1a} + \lambda_1)\exp(\lambda_1 t) - (k_{-1a} + \lambda_2)\exp(\lambda_2 t)}{\lambda_1 - \lambda_2} \quad (3)$$

where S_t is the total signal at time t, the background is a constant arising from scattered light, S_0 is the LIF intensity at $t = 0$, and λ_1 and λ_2 are given by

$$\lambda_{1,2} = \frac{-a \pm \sqrt{a^2 - 4k_d k_{-1a}}}{2}$$

where $a = k_{-1a} + k_d + k_{1a}[CH_2CCl_2]$.

The decays at 680 K were analyzed as follows with a resulting fit shown in Figure 11. First, k_d was fixed from a run with $[CH_2CCl_2] = 0$ by a fit of S_t to a simple exponential decay plus background. The remaining decays were fit directly to eq 3 with the background, S_0, and k_{-1a} as the only adjustable parameters. k_1 was set to 3.84×10^{-12} cm^3 $molecule^{-1}$ s^{-1} from a small extrapolation of the Arrhenius expression derived for 291−640 K. k_{-1a} is not determined very precisely: the derived k_{-1a} values range from 1000 to 2100 s^{-1} and their mean is 1550 ± 510 s^{-1} ($\pm 2\sigma$ of the mean), but these data do permit precise determination of the adduct binding energy. The concentration equilibrium constant for the adduct formation channel 1a, $K_c = k_{1a}/k_{-1a}$, is 2.5×10^{-15} cm^3 $molecule^{-1}$ at 680 K. Relative to a standard state of 10^5 Pa, $K_{eq} = 2.6 \times 10^4$. Use of $\Delta S = -28.2$ cal K^{-1} mol^{-1} derived from the data in Table 7, together with $\Delta G = -RT \ln K_{eq} = \Delta H - T\Delta S$, implies $\Delta H = -32.9$ kcal mol^{-1}. We allow for a factor of 3 uncertainty in K_{eq} to obtain error limits of ± 1.5 kcal mol^{-1}.

Correction of this ΔH to 298 K and using the C_p data (Table 7) yields a C−O bond dissociation enthalpy (BDE) of 32.8 ± 1.5 kcal mol^{-1}. This corresponds to a 0 K value of 31.9 ± 1.5 kcal mol^{-1}. An independent test of the BDE for OH + 1,1-dichloroethylene effect comes from the data of Table 3, which imply $BDE_{298} = 31.3$ kcal mol^{-1}. These values are somewhat larger than the BDE determined by Fulle et al.[31] for the analogous OH + ethylene adduct, of 29.4 ± 1.4 kcal mol^{-1} at 0 K. Apparently, chlorine substitution stabilizes to a small degree the radical center in the adduct.

Summary

New atmospheric pressure, absolute rate measurements are presented for the reaction of OH radicals with 1,1-dichloroethylene (k_1) and *trans*-1,2-dichloroethylene (k_2). The new kinetic measurements (and modeling results) are consistent with prior lower temperature measurements for both substrates. The data for k_1 (below 640 K) and k_2 were successfully modeled by conducting an ab initio based reaction pathway analysis based on an OH addition mechanism. Variational TST calculations of the entrance channel were consistent with the experimental measurements for k_1 but incorrectly predict a significant barrier for addition of OH to *trans*-1,2-dichloroethylene. The reason for the discrepancy for the second reaction is unclear. Adduct stabilization was found to be the dominant mechanism for 1,1-dichloroethylene below 700 K, hence, the observed negative temperature-dependence. Analysis of equilibration in this system yields a C−O bond dissociation enthalpy of 32.8 ± 1.5 kcal mol^{-1} at 298 K, a value confirmed by ab initio calculations. Cl elimination was found to be the dominant mechanism for *trans*-1,2-dichloroethylene at all temperatures. Ab initio based TST calculations for the respective H-atom abstraction channels indicated that this mechanism is important at temperatures above 700 and 800 K for k_1 and k_2, respectively. At flame temperatures,

H atom abstraction will be the dominant mechanism of OH attack for both substrates.

Just prior to submitting this manuscript for publication, we became aware of a recently published room temperature study of the OH-initiated oxidation of the chlorinated ethylenes.[32] This experimental study, using the discharge-flow technique, also reported measurements of Cl atom production following the OH-initiated reaction. For 1,2-dichloroethylene, the room temperature chlorine atom yield was essentially unity, whereas for 1,1-dichloroethylene, the chlorine atom yield was essentially zero. The Cl atom yields and the room-temperature rate constants for OH reaction with 1,1- and 1,2-dichloroethylene are consistent with the experimental data and mechanistic analysis presented herein.

Acknowledgment. The authors acknowledge support from the Environmental Protection Agency (Grant R82-6169-01-0). Although this research has been supported by the US-EPA, it has not been subject to Agency review and therefore does not necessarily reflect the views of the Agency, and no official endorsement should be inferred. P.M. also thanks the R.A. Welch Foundation (Grant B-1174) and UNT for support. Some of the calculations were performed on the National Computational Science Alliance SGI/Cray Origin 2000 (Grant CHE000015N) and at facilities generously provided by the Materials and Manufacturing Division of the Air Force Research Laboratory at Wright-Patterson AFB, Ohio.

Supporting Information Available: Table 1S and 2S present computed molecular geometries and vibrational frequencies for reactants, intermediate radicals, transition states, and products except OH and H_2O. This material is available free of charge via the Internet at http://pubs.acs.org.

References and Notes

(1) Kirchner, K.; Helf, D.; Ott, P.; Vogt, S. *Ber. Bunsen-Ges. Phys. Chem.* **1990**, *94*, 77.

(2) Ramamoorthy, S.; Ramamoorthy, S. *Chlorinated Organic Compounds in the Environment*; Lewis Publishers: New York, 1997; Chapter 3.

(3) Fairchild, P. W.; Smith, G. P.; Crosley, D. R. *Proc. Combust. Inst.* **1982**, *19*, 107.

(4) Warnatz, J.; Bockhorn, H.; Moser, A.; Wenz, H. W. *Proc. Combust. Inst.* **1982**, *19*, 197.

(5) Edney, E. O.; Kleindienst, T. E.; Corse, E. W. *Int. J. Chem. Kinet.* **1986**, *18*, 1355.

(6) Tuazon, E. C.; Atkinson, R. A.; Aschmann, S. M.; Goodman, M. A.; Winer, A. M. *Int. J. Chem. Kinet.* **1988**, *20*, 241.

(7) Zhang, Z.; Liu, R.; Huie, R. E.; Kurylo, M. J. *J. Phys. Chem.* **1991**, *95*, 194.

(8) Abbatt, J. P. D.; Anderson, J. G. *J. Phys. Chem*. **1991**, *95*, 2382.

(9) Atkinson, R. *J. Phys. Chem. Ref. Data* **1989**, Monograph 1.

(10) Tichenor, L. B.; Taylor, P. H.; Yamada, T.; Peng, J.; Hu, X.; Marshall, P. *J. Phys. Chem. A.* **2000**, *104*, 1700.

(11) Tichenor, L. B.; El-Sinawi, A.; Taylor, P. H.; Yamada, T.; Peng, J.; Hu, X.; Marshall, P. *Chemosphere* **2001**, *42*, 571.

(12) Tichenor, L. B.; Lozada-Ruiz, A. J.; Yamada, T.; El-Sinawi, A.; Taylor, P. H.; Peng, J.; Hu, X.; Marshall, P. *Proc. Combust. Inst.* **2000**, *28*, 1495.

(13) Febo, A.; Perrino, C.; Gherardi, M.; Sparapani, R. *Environ. Sci. Technol.* **1995**, *29*, 2390.

(14) Brust, A. S.; Becker, K. H.; Kleffmann, J.; Wiesen, P. *Atmos. Environ.* **2000**, *34*, 13.

(15) Wollenhaupt, M.; Carl, S. A.; Horowitz, A.; Crowley, J. N. *J. Phys. Chem.* **2000**, *104*, 2695.

(16) Cox, R. A. *J. Photochem.* **1974**, *3*, 175.

(17) Curtiss, L. A.; Redfern, P. C. *J. Chem. Phys.* **1999**, *110*, 4703−4709.

(18) Frisch, M. J.; Trucks, G. W.; Schlegel, H. B.; Gill, P. M. W.; Johnson, B. G.; Robb, M. A.; Cheeseman, J. R.; Keith, T.; Petersson, G. A.; Montgomery, J. A.; Raghavachari, K.; Al-Laham, M. A.; Zakrzewski, V. G.; Ortiz, J. V.; Foresman, J. B.; Cioslowski, J.; Stefanov, B. B.; Nanayakkara, A.; Challacombe, M.; Peng, C. Y.; Ayala, P. Y.; Chen, W.; Wong, M. W.; Andres, J. L.; Replogle, E. S.; Gomperts, R.; Martin, R. L.; Fox, D. J.; Binkley, J. S.; Defrees, D. J.; Baker, J.; Stewart, J. P.; Head-Gordon, M.; Gonzalez, C.; Pople, J. A. *Gaussian 94*; Gaussian, Inc.: Pittsburgh, PA, 1995

(19) Frisch, M. J.; Trucks, G. W.; Schlegel, H. B.; Scuseria, G. E.; Robb, M. A.; Cheeseman, J. R.; Zakrzewski, V. G.; Montgomery, J. A., Jr.; Stratmann, R. E.; Burant, J. C.; Dapprich, S.; Millam, J. M.; Daniels, A. D.; Kudin, K. N.; Strain, M. C.; Farkas, O.; Tomasi, J.; Barone, V.; Cossi, M.; Cammi, R.; Mennucci, B.; Pomelli, C.; Adamo, C.; Clifford, S.; Ochterski, J.; Petersson, G. A.; Ayala, P. Y.; Cui, Q.; Morokuma, K.; Malick, D. K.; Rabuck, A. D.; Raghavachari, K.; Foresman, J. B.; Cioslowski, J.; Ortiz, J. V.; Stefanov, B. B.; Liu, G.; Liashenko, A.; Piskorz, P.; Komaromi, I.; Gomperts, R.; Martin, R. L.; Fox, D. J.; Keith, T.; Al-Laham, M. A.; Peng, C. Y.; Nanayakkara, A.; Gonzalez, C.; Challacombe, M.; Gill, P. M. W.; Johnson, B. G.; Chen, W.; Wong, M. W.; Andres, J. L.; Head-Gordon, M.; Replogle, E. S.; Pople, J. A. *Gaussian 98*, revision x.x; Gaussian, Inc.: Pittsburgh, PA, 1998.

(20) Stull, D. R.; Westrum, E. F., Jr.; Sinke, G. C. *The Chemical Thermodynamics of Organic Compounds*; John Wiley & Sons: New York, 1969.

(21) Stull, D. R.; Prophet, H. *JANAF Thermochemical Tables*, NSRDS−NBS 37; U. S. Government Printing Office: Washington, DC, 1971.

(22) Mansson, R.; Ringer, B.; Sunner, S. *J. Chem. Thermodyn.* **1971**, *3*, 547.

(23) Hehre, W. J.; Radom, L.; Schleyer, P. R.; Pople, J. A. *Ab Initio Molecular Orbital Theory*; John Wiley & Sons: New York, 1986.

(24) Pitzer, K. S.; Gwinn, W. *J. Chem. Phys.* **1942**, *10*, 428.

(25) Benson, S. W. *Thermochemical Kinetics*; Wiley-Interscience: New York, 1976.

(26) Westmoreland, P. R. *Combust. Sci. Technol.* **1992**, *82*, 151−168.

(27) Bozzelli, J. W.; Dean, A. M.; Ritter, E. R. *Combust. Sci. Technol.* **1991**, *80*, 63.

(28) Gilbert, R. G.; Luther, K.; Troe, J. *Ber. Bunsen-Ges. Phys. Chem.* **1983**, *87*, 169.

(29) Ochterski, J. W.; Petersson, G. A.; Montgomery, J. A., Jr. *J. Chem. Phys*. **1996**, *104*, 2598.

(30) Ayhens, Y. V.; Nicovich, J. M.; McKee, M. L.; Wine, P. H. *J. Phys. Chem. A* **1997**, *101*, 9382.

(31) Fulle, D.; Hamann, H. F.; Hippler, H.; Jänsch, C. P. *Ber. Bunsen-Ges. Phys. Chem.* **1997**, *101*, 1435.

(32) Canosa-Mas, C. E.; Dillon, T. J.; Sidebottom, H.; Thompson, K. C.; Wayne, R. P. *Phys. Chem. Chem. Phys.* **2001**, *3*, 542.

(33) Barat, R. B.; Bozzelli, J. W. *J. Phys. Chem.* **1992**, *96*, 2494.